Anomalous collapse of interacting bubbles in a fluidized bed: A magnetic resonance imaging study

C. M. Boyce,[1,2,*] A. Penn,[1,3] A. Padash,[2] M. Lehnert,[1] K. P. Pruessmann,[3] and C. R. Müller[1]
[1]*Department of Mechanical and Process Engineering, ETH Zurich, 8092 Zurich, Switzerland*
[2]*Department of Chemical Engineering, Columbia University, New York, New York 10027, USA*
[3]*Institute for Biomedical Engineering, ETH Zurich and University of Zurich, 8006 Zurich, Switzerland*

(Received 12 October 2018; published 18 March 2019)

The collapse, or reduction in size to zero volume, of bubbles injected into incipiently fluidized beds was studied using rapid magnetic resonance imaging. The collapse of a smaller lower bubble trailing a larger upper bubble and the collapse of one bubble when two bubbles rose side by side were found to occur. Under the same conditions with the use of finer particles or the injection of an isolated bubble, no collapse occurred. Thus, results indicate that gas leakage into the particulate phase of coarse particles and bubble interaction promote bubble collapse. Furthermore, injection of larger bubbles also resulted in bubbles rising to the bed surface instead of collapsing, indicating that bubbles must be below a critical size in order to collapse. For side-by-side bubbles, bubble collapse is attributed to gas flow channeling to the larger bubble; for consecutive bubbles, bubble collapse is attributed to increased gas leakage in a dilated bubble wake.

DOI: 10.1103/PhysRevFluids.4.034303

I. INTRODUCTION

Gas bubbles in fluidized beds have fascinated researchers for decades due to their apparent similarities to, but also large differences from, gas bubbles in liquids. Gas bubbles in fluidized beds are notably different from those in liquids since there is no surface tension at the interface between the bubble and particulate phases and gas flows freely through this interface as gas travels both in bubbles and in between the interstices between particles. Despite these critical differences, the rise velocity and shape of bubbles in fluidized beds are similar to those in liquids. Due to these interesting physical aspects and the relevance of gas bubbles in fluidized beds to industrial processes in inducing particle mixing but also limiting gas-solid contact, several studies have investigated the stability of bubbles in fluidized beds [1,2]. Previous studies have shown bubbles to split up [2] and coalesce [3,4] in many systems and, in rarer cases, studies have found bubbles to collapse (i.e., disappear, become extinct, or reduce to zero volume) and spawn in the midst of fluidized particles [5,6]. Due to the rarity of reports of bubble collapse, most stability studies have focused on a maximum bubble size achieved in a fluidized bed [1,2] caused by a competition between bubble coalescence promoting growth and bubble splitting promoting shrinkage.

Certain cases of bubble collapse can be explained via a change in system parameter. For example, a decrease in superficial gas velocity can defluidize the bed or cause it to enter a homogeneous fluidization regime [7], resulting in the collapse of bubbles. Alternatively, an increase in gas flow rate can cause the bed to enter a fast fluidization regime, in which an upward flow of particles occurs without the persistence of bubbles [8]. Additionally, vibrating a fluidized bed has been shown to result in the collapse of gas voids in certain cases [9].

*Corresponding author: cmb2302@columbia.edu

While explaining the physics of bubble collapse due to a change in flow parameters is often straightforward, there are other cases in which bubbles disappear without any flow parameters changing [5,6]. This type of collapse of bubbles is often a perplexing phenomenon since it is frequently approximated that all gas flow in excess of that necessary to fluidize the particles travels through the bed in the form of bubbles [10]. However, previous work [11] has shown that this approximation is fairly inaccurate, and a significant amount of excess gas flow goes into interstitial flow rather than bubbles, especially in the case of coarse particles in group D according to Geldart's classification [12]. Thus, bubble collapse could be explained via gas leakage from bubbles into the interstitial phase. Bubble collapse has been reported in pseudo-two-dimensional beds with solid circular obstacles [5], indicating that passage around obstacles could facilitate collapse. Additionally, bubble collapse has been seen in fluidized beds with low excess gas velocities [6], and has been attributed to defluidization of regions below and to the sides of bubbles at these low excess gas velocities [13], resulting in unusual behavior.

Here, we report and investigate the collapse of bubbles in the wake of leading bubbles and bubbles to the side of another bubble when two bubbles are injected into an incipiently fluidized bed. We conduct the experiments in a three-dimensional (3D) cylindrical fluidized bed and characterize the solids volume fraction and particle velocity field using rapid magnetic resonance imaging (MRI). These recently developed MRI capabilities [14] have been used to characterize bubble motion in freely bubbling beds [15,16], as well as single bubbles injected into incipiently fluidized beds [17–19] and the interaction of jets injected into incipiently fluidized beds [20]. Here, we study bubble behavior in beds with particles of different sizes and different arrangements of bubble injection in order to illuminate the roles of gas leakage and bubble interaction on bubble collapse.

II. METHODS

A. Fluidized bed

A cylindrical fluidized bed was used with a diameter of 190 mm and a height of 300 mm. Particles filled the bed to a height of $H_0 = 200$ mm, and the particles were fluidized by air at ambient conditions. The distributor was a 10 mm perforated plate made of polymethyl methacrylate (PMMA). The particles were incipiently fluidized, such that no bubbles formed other than those injected into the bed through orifices. Agar shells filled with oil were used as fluidized particles since an MRI signal arises from the oil within them. Particles of two different sizes were used in separate experiments: particles with diameter $d_p = 1.02 \pm 0.12$ and 2.93 ± 0.04 mm, hereon referred to as 1 and 3 mm particles, respectively. The 1 mm particles had a density of $\rho_p = 1040\,\mathrm{kg/m^3}$, a coefficient of friction of $\mu = 0.54 \pm 0.05$, and a coefficient of restitution of $\mathrm{e} = 0.70 \pm 0.03$. The 3 mm particles had very similar properties: $\rho_p = 1040\,\mathrm{kg/m^3}$, $\mu = 0.56 \pm 0.04$, and $e = 0.69 \pm 0.03$. The 3 mm particles were Geldart group D and 1 mm particles were on the border between group B and D classifications [12], The minimum fluidization velocities of the 1 and 3 mm particles were 0.25 and 0.70 m/s, respectively.

B. Bubble injection

Bubble injection ports 7.95 mm in diameter and flush with the distributor were used to inject bubbles into incipiently fluidized beds. Two configurations of ports were used: (1) a single central port and (2) two ports separated by 80 mm, each 40 mm from the center of the distributor. Air was injected from a 2.5 L tank kept at 3.0 bar g for finite periods of time using solenoid valves (SMC VQ20 series). The time of injection was controlled by opening the valves for a specified amount of time using an interface with LABVIEW. The injection times and the corresponding volume of air injected are shown in Table 1; for the range of injection times used here, the relationship between injection time and injected air volume was linear.

TABLE I. Bubble injection times and volumes.

Injection Time (ms)	Injection Volume (L)
75	0.48
50	0.37
40	0.33
30	0.24
25	0.18

C. MRI measurements

A Philips Achieva 3T medical scanner with a custom-built 16-channel radio-frequency array [14] was used to detect the magnetic resonance signal arising from oil within the particles. Echo planar imaging (EPI) [21] was used to measure the particle concentration field with a temporal resolution of 7.17 ms and a nominal spatial resolution of 3 mm horizontal (x) $\times$ 3 mm vertical (y). Echo planar imaging with phase contrast velocimetry [22] was used to measure both the solids volume fraction and the vertical and horizontal components of the particle velocity with a temporal resolution of 18 ms and a nominal spatial resolution of 3 mm horizontal (x) $\times$ 5 mm vertical (y). The phase contrast velocimetry used here is based on ensemble averaging of the displacement of particles during the observation period ($\Delta = 0.55$ ms) between the centers of two bipolar flow-encoding pulsed field gradients imparting a phase change on the received signal proportional to the displacement distance. The velocity is taken as the displacement divided by the observation period. For each velocity image produced, three excitations and signal acquisitions, each taking 6 ms, are used, one with flow encoding gradients in the horizontal direction, one with gradients in the vertical direction, and one without flow-encoding gradients to provide a baseline for phase shift. For both types of measurements, a central vertical slice through the bed with a thickness of 10 mm was taken and the field of view was 200 mm (x) $\times$ 300 mm (y). The MRI pulse sequences used in this work are detailed and discussed in [14].

D. Determination of bubble volumes

Figure 1 shows how maps of solid volume fraction were used to determine bubble volumes. Figure 1 shows a raw image of the solids concentration [Fig. 1(a)] and the conversion of that raw image into a binary image [Fig. 1(b)] where a pixel is either in the bubble or gas phase based on

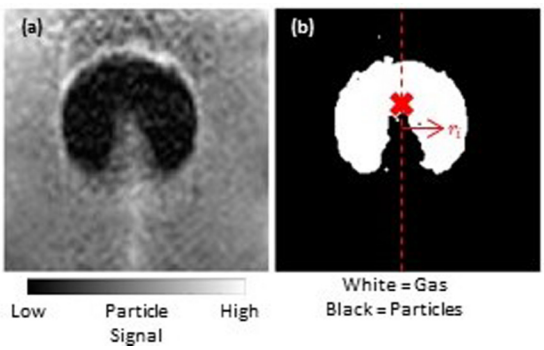

FIG. 1. Schematic of the process for determining bubble volume: (a) raw image of particle concentration field; (b) binary image of gas and particulate pixels after applying a signal threshold to (a). The centroid of the bubble in (b) is shown with a red $\times$, and this is used to draw the vertical center line. The bubble volume is determined based on the radius of each gas pixel from the center line and assuming axis symmetry.

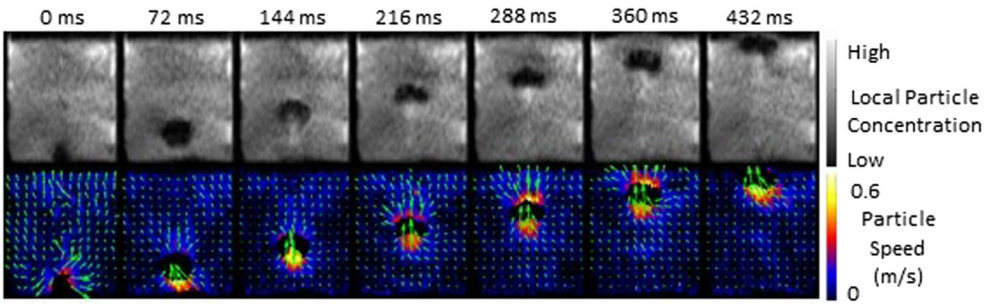

FIG. 2. Time series of images of local particle concentration (upper row) and local particle velocity (lower row) for single bubbles injected into incipiently fluidized beds of 3 mm particles for an injection time of 25 ms. Green arrows indicate the direction of particle velocity.

the use of a threshold for the signal in Fig. 1(a). The threshold makes it such that any pixel with a signal greater than 18% of that of the pixel with the maximum signal is considered to be part of the particulate phase and any pixel below this threshold is part of the gas phase. Via binary image processing, the centroid of the bubble was determined based on the center of the gas pixels. As shown in Fig. 1(b), the horizontal distance r_i of each pixel i from the centroid of the bubble was determined and this distance was used to calculate the volume of the bubble, assuming the bubble is axis symmetric about the vertical axis,

$$V_b = \sum_{i=1}^{N_{\text{pixels,gas}}} \pi r_i dx dy, \tag{1}$$

where $dx = 1$ mm $dy = 1$ mm are the width and height of each pixel, respectively.

E. Determination of bubble rise velocity

The bubble rise velocity was determined using a linear regression through the data for the vertical position of the centroid of the bubble over time. The rise velocity was the slope of the linear regression.

III. RESULTS AND DISCUSSION

The quantitative data shown here are provided in the form of MATLAB files and scripts for the convenience of those seeking to make a direct comparison with analytical theory, numerical simulations, or other experiments.

A. Single-bubble injection

Figure 2 shows a time series of images of a single injected bubble rising through an incipiently fluidized bed with a bubble injection time of 25 ms. The upper row shows images of particle signal intensity and the lower row shows the corresponding maps of particle velocity. The images are taken through a central slice of the fluidized bed. Figure 2 shows that an isolated bubble rises to the surface of the bed without collapsing. The particle velocity below the bubble in its "wake" and above the bubble in its "crown" is highest, with upward particle velocities approximately matching the rise velocity of the bubble, $u_b = 0.5$ m/s. Particles to the side of the bubble move downwards to replenish the particles carried up with the bubble. The bubble starts out in a spherical shape when it detaches from the injection orifice, but develops into a spherical-cap shape as it rises. As confirmed quantitatively in Fig. 3, the bubble appears to become slightly smaller in volume as it rises to the center of the bed, but then increases in volume as it approaches the bed surface.

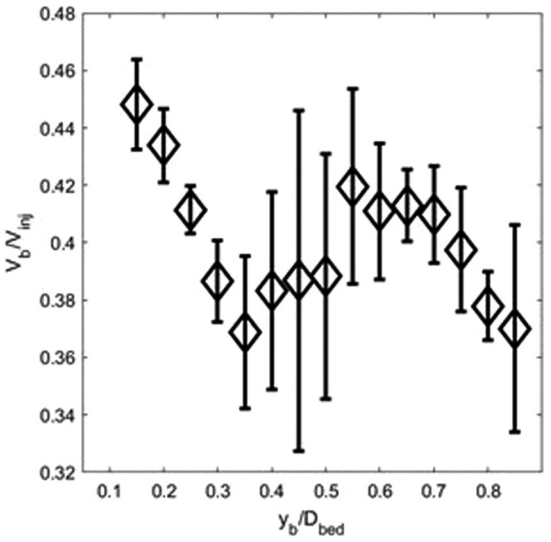

FIG. 3. Bubble volume normalized by volume injected vs normalized vertical position of the centroid of the bubble for an injection time of 25 ms into an incipiently fluidized bed of 3 mm particles. Error bars show the standard deviation from three measurements.

Figure 3 shows the bubble volume normalized by the injected gas volume versus the vertical position of the centroid of the bubble normalized by the bed diameter for an isolated bubble with a 25 ms injection time into an incipiently fluidized bed of 3 mm particles. At all vertical positions, the bubble volume is significantly lower than the amount of air injected; this can be attributed to gas leakage into the interstitial flow during injection [23]. As seen in Fig. 2, the bubble initially decreases in volume low in the bed, then increases in volume in the middle of the bed, and then decreases in volume toward the bed surface. These trends can be attributed perhaps to different rates of gas leakage and absorption from the interstitial flow as the bubble develops in shape and moves through different regions of the bed; these unusual aspects of absorption and leakage at low superficial gas velocities have been reported previously [13]. Although the bubble oscillated in volume, in three experiments with an injection time of 25 ms, an isolated bubble never came close to collapsing (reaching a volume of zero).

B. Two bubbles injected side by side

Figure 4 shows a time series of the particle signal images of two bubbles injected simultaneously from two ports separated by 80 mm. The time series for different injection times and different particle sizes are shown in different rows. For 1 mm particles, the two bubbles rise without coalescing and develop from a spherical shape initially into a spherical-cap shape as they rise. The two bubbles are similar in size and shape to one another throughout the rising process. The same trend is observed for 3 mm particles with a 40 ms injection time. For 3 mm particles with an injection time of 30 ms, the two bubbles are similar in size initially, but over time the left bubble decreases in size until it fully collapses before reaching the bed surface. In contrast, the right bubble maintains its size throughout the rise process and reaches the bed surface without collapsing. These results indicate that under certain conditions, gas leakage and transfer effects between side-by-side bubbles can lead to the collapse of bubbles. In contrast, single bubbles injected into beds of 3 mm particles with injection times of 25 and 50 ms do not collapse, as shown for $t_{inj} = 25$ ms in Fig. 2, indicating that bubble interaction plays a role in bubble collapse. The fact that bubble collapse does not occur in 1 mm particles can be attributed to the fact that there is less gas leakage into the interstitial flow

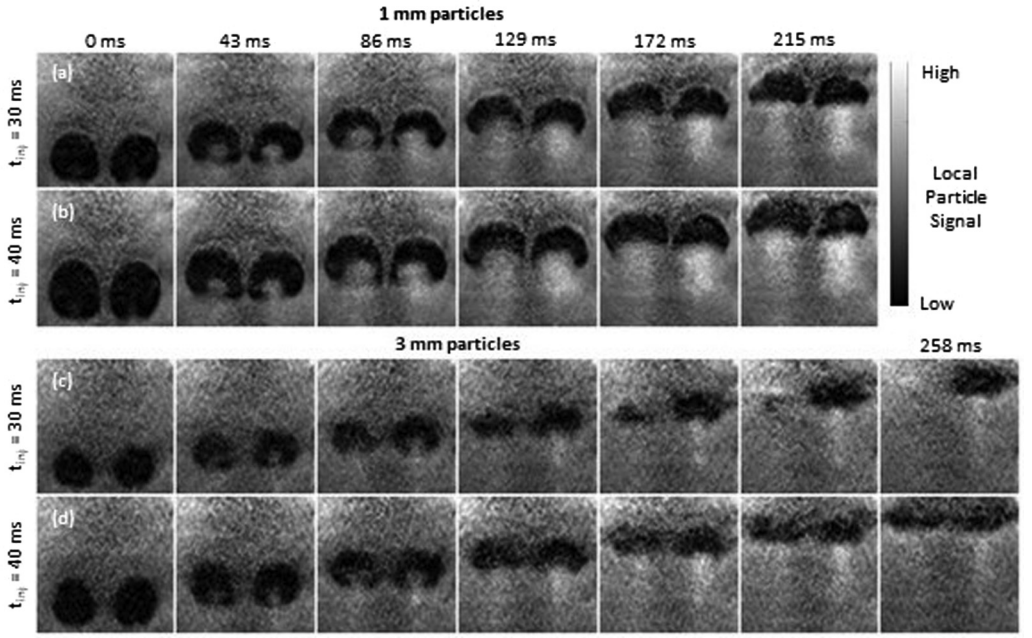

FIG. 4. Time series of signal intensity images for two bubbles injected side by side into (a) 1 mm particles with $t_{\text{inj}} = 30$ ms, (b) 1 mm particles with $t_{\text{inj}} = 40$ ms, (c) 3 mm particles with $t_{\text{inj}} = 30$ ms, and (d) 3 mm particles with $t_{\text{inj}} = 40$ ms.

during bubble injection [23] and, as the bubbles rise, due to the lower permeability ($k \propto d_p^3$) of small particles to interstitial gas flow [24].

Figure 5 quantifies the results shown in Fig. 3 for 1 mm particles [Fig. 5(a)] and 3 mm particles [Fig. 5(b)]. For 1 mm particles, the normalized volumes of both bubbles are fairly similar to one another throughout the rising process; the two bubbles decrease in size as they rise due to gas leakage into the interstitial flow, but both reach the surface without collapsing. Figure 5(c) shows that while the volume of the individual bubbles may vary somewhat, the total normalized bubble volume (the sum of the volumes of the left and right bubbles) is fairly similar for the 30 and 40 ms injection times throughout the bubble rise process. The same trend of left and right bubbles maintaining similar volumes and reaching the bed surface without collapsing is observed for 3 mm particles with a 40 ms injection time. In contrast, for 3 mm particles with an injection time of 30 ms, the left bubble rapidly decreases in volume until it has no more volume at approximately $y_b/D_{\text{bed}} = 0.5$. As the left bubble rapidly decreases in volume, the right bubble approximately maintains its volume and only shows a significant decrease in volume after the left bubble has collapsed. These results indicate that gas leaks from the left bubble not only into the interstices between particles, but that gas is also transferred into the right bubble to help it to maintain its volume. After the left bubble has collapsed, there is no gas left to transfer into the right bubble, and thus the right bubble begins to lose volume due to gas leakage into the interstitial flow. The sum of volumes of the left and right bubble for 3 mm particles in Fig. 5(d) show that despite the collapse of the left bubble for the 30 ms injection-time case, the total normalized bubble volume is fairly similar throughout the rise process for both the 30 and 40 ms injection times. The only point at which the two cases with different injection times differs comes at $y/D_{\text{bed}} = 0.5$, just after the left bubble has collapsed in the 30 ms injection case and the total bubble volume for this case is significantly lower than that in the 40 ms case. However, by a position of $y/D_{\text{bed}} = 0.7$, the total normalized bubble volumes for the 30 and 40 ms cases are again similar to one another. These results indicate that gas leaks into the interstices

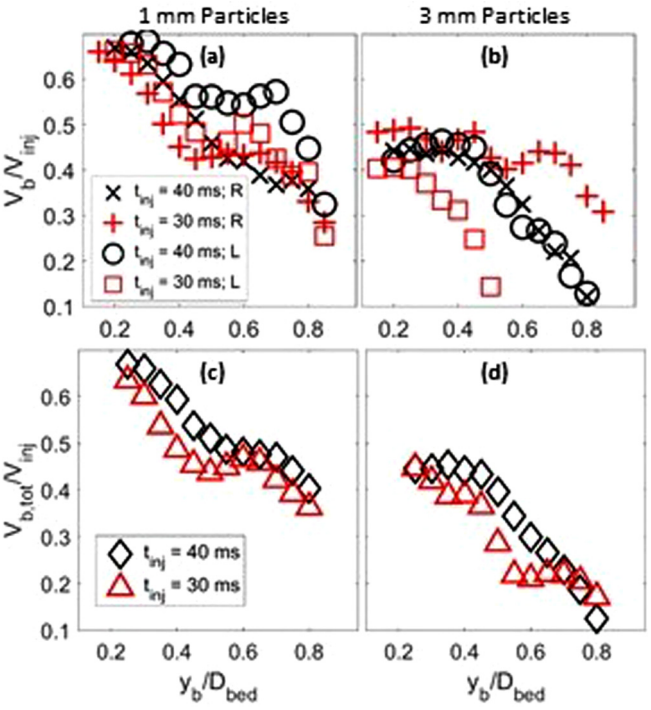

FIG. 5. Normalized bubble volume vs vertical position of the centroid of the bubble for two bubbles injected side by side (L = left, R = right) into an incipiently fluidized bed of (a) 1 mm particles and (b) 3 mm particles. (c),(d) The total normalized bubble volume from both the right and left bubbles in (a) and (b), respectively.

between particles as the left bubble collapses and there is a transient period when gas, perhaps that from the collapsed bubble, is absorbed by the right bubble from $y/D_{\text{bed}} = 0.5-0.7$. Eventually the volume of gas which would otherwise still exist in the left bubble is fully absorbed into the right bubble.

It is important to define exactly what we are referring to as "collapse" versus "coalescence" in this paper, especially since the results of Figs. 4 and 5 indicate a transfer of gas from one bubble to another. By collapse we are referring to the volume of a bubble reaching zero without its surface reaching the surface of another bubble such that the two bubbles overlap in space. Even if the gas originally within a collapsed bubble is absorbed into the volume of another bubble after passing through the particulate phase, this does not constitute coalescence in our definition. Coalescence occurs only when two bubbles overlap in space causing them to merge into one bubble.

The authors are unaware of other reports in the literature of bubble collapse due to interaction between side-by-side bubbles. Thus, Fig. 6 seeks to further illuminate this phenomenon by providing a time series of images of particle signal intensity (upper row) and particle velocity (lower row) for 30 ms injection times in beds of 1 mm [Fig. 6(a)] and 3 mm [Fig. 6(b)] particles. For the 1 mm particles, as both bubbles rise, they have faster particle velocities below them than above them, and thus the bubbles evolve from a spherical to a spherical-cap shape. However, for the 1 mm particles, the particle velocities are still high enough above the bubble for the roof of the bubble to maintain its shape as the bubble rises. In contrast, for the 3 mm particles, the left bubble rises, but there is almost no upward motion of particles above the bubble, and thus the particles in the wake reach the bubbles in the roof of the bubble, causing it to collapse. This mechanism is consistent with the flow of gas through the roof of the left bubble being too slow to support the particles at its roof as it rises. One possible reason for this is that if the right bubble is slightly larger than the left bubble initially,

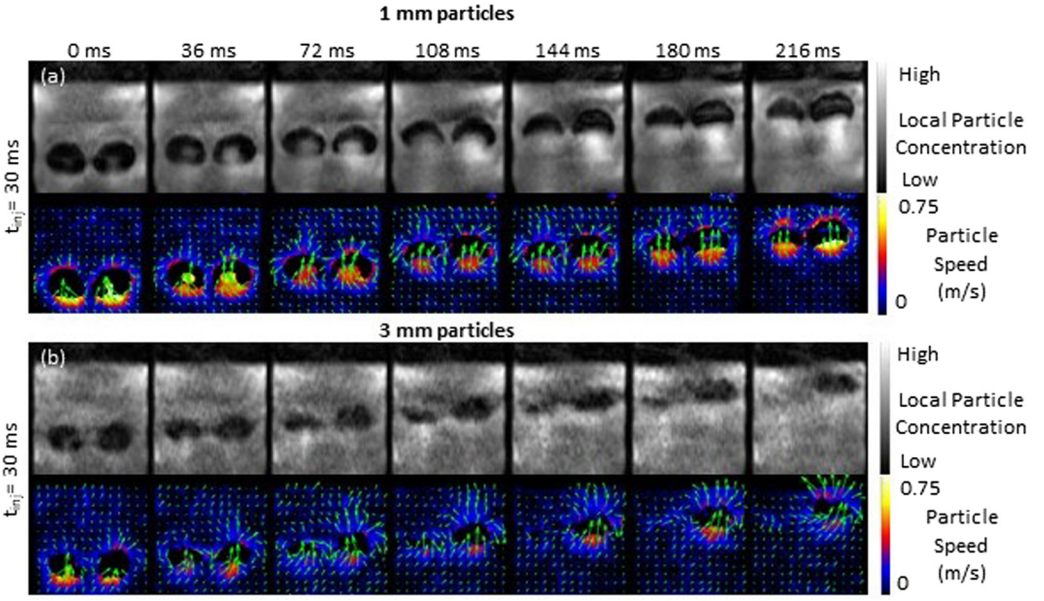

FIG. 6. Time series of images particle signal intensity (upper row) and particle velocity (lower row) for side-by-side bubbles in incipiently fluidized beds of (a) 1 mm particles and (b) 3 mm particles with injection times of 30 ms.

more gas will channel through the right bubble, as shown schematically in Fig. 7, causing the flow through the left bubble to be insufficient to support it. The lower permeability of gas flow through 1 mm particles and the lower gas flow needed to support a roof of 1 mm particles prevents the rapid growth of this instability in small particles, and thus no bubble collapse is observed.

In repetitions of the experiment with 3 mm particles and 30 ms injection times, sometimes the left bubble collapses and sometimes the right bubble collapses. In contrast, for all of the other cases shown in Fig. 4, both bubbles survive to reach the bed surface in all repetitions of the experiment. These trends indicate that the bubble collapse is indeed the manifestation of an instability, rather than an issue with the experimental setup.

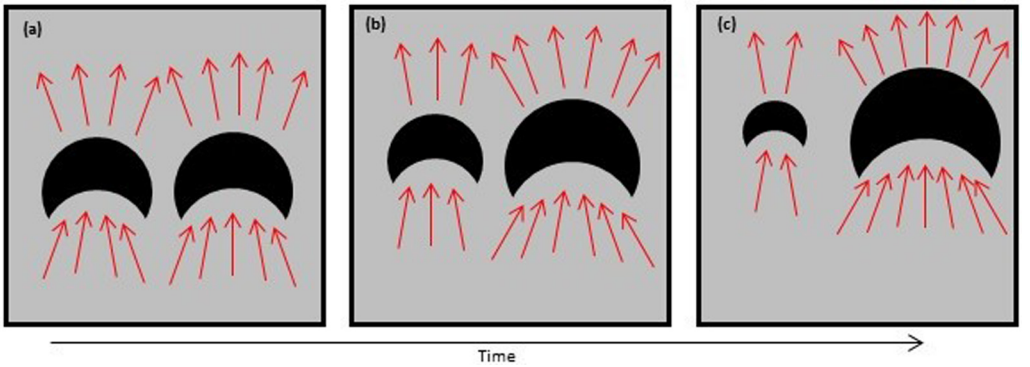

FIG. 7. Schematic showing gas flow (red arrows) through side-by-side bubbles, leading to the larger bubble growing due to gas channeling through it, while the smaller bubble decreases in volume due to gas channeling away from it.

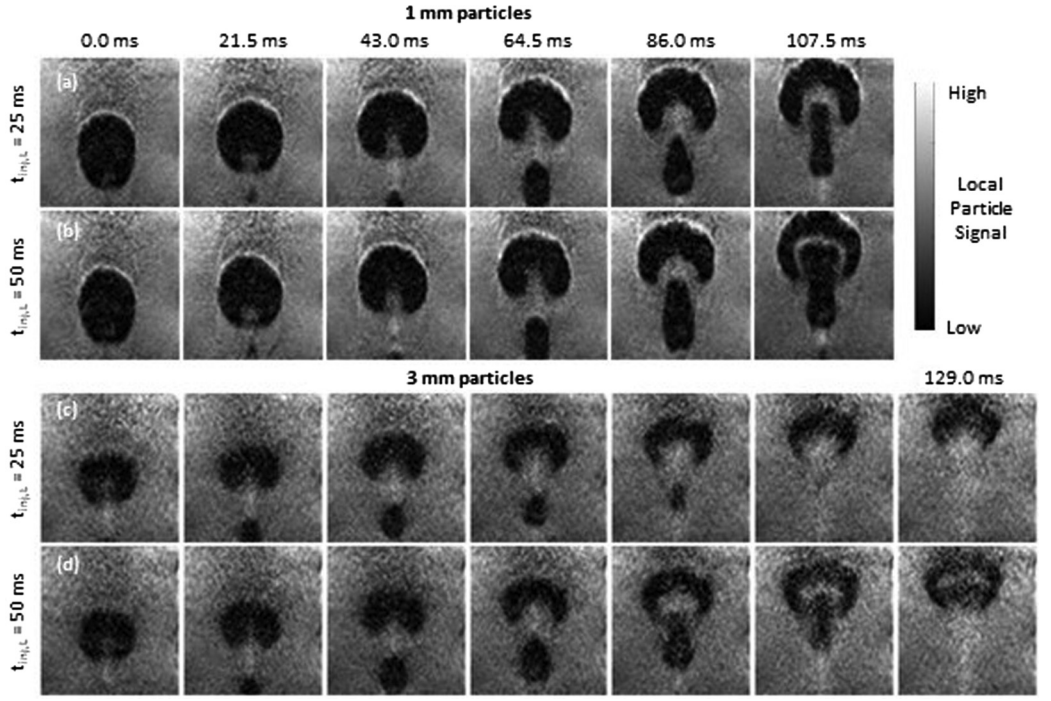

FIG. 8. Time series of signal intensity images for two bubbles injected consecutively into incipiently fluidized beds with an injection time of $t_{\mathrm{inj},U} = 75$ ms for the first injection and a separation time between injections of $t_{\mathrm{sep}} = 50$ ms. Different values for particle diameter and injection time of the lower bubble were used: (a) $t_{\mathrm{inj},L} = 50$ ms, 1 mm particles; (b) $t_{\mathrm{inj},L} = 25$ ms, 1 mm particles; (c) $t_{\mathrm{inj},L} = 50$ ms, 3 mm particles; and (d) $t_{\mathrm{inj},L} = 25$ ms, 3 mm particles.

C. Two bubbles injected consecutively

Figure 8 shows the time series of images of particle signal intensity for two bubbles injected consecutively through a central orifice into incipiently fluidized beds. The injection time of the first bubble is 75 ms and the separation time between bubble injections is 50 ms. Different rows show the image series for different particle sizes as well as different injection times for the lower bubble. For the 1 mm particles, the upper bubble develops in shape as it rises from a spherical shape to a spherical-cap shape, similar to a single injected bubble. The lower bubble, however, is clearly influenced by the upper bubble and forms a vertically elongated shape as it approaches the upper bubble for coalescence. The same trends are observed in the 3 mm particles with a lower bubble injection time of 50 ms. However, for 3 mm particles with a lower bubble injection time of 25 ms, a different type of behavior is observed. The lower bubble initially rises with a vertically elongated shape as in the other cases shown; however, it is much smaller than the bubbles in the other cases and eventually collapses without coalescing with the upper bubble. The bubble is much smaller [see Fig. 9(b)] than the single-bubble injection with an injection time of 25 ms, shown in Fig. 2, which reaches the surface of the bed without collapsing. These results indicate that gas leakage and wake effects for a trailing bubble can lead to bubble collapse, another phenomenon the authors have not been able to find reported in the literature.

Figure 9 shows the normalized bubble volume versus vertical position of the bubble for upper and lower bubbles for consecutive bubble injections with different lower bubble injection times and particle sizes of 1 mm [Fig. 9(a)] and 3 mm [Fig. 9(b)]. For all cases, the upper bubble injection time is 75 ms and the separation time between bubble injections is 50 ms. The figure shows that the

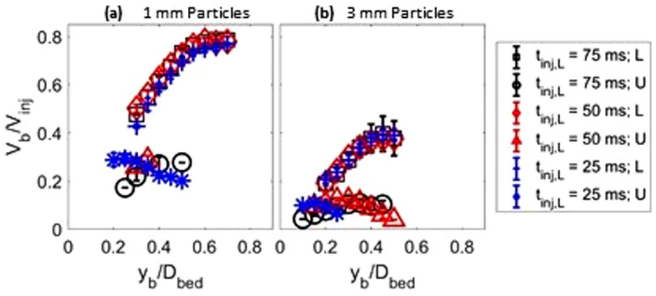

FIG. 9. Normalized bubble volume vs normalized vertical position of the bubble for upper (U) and lower (L) bubbles for consecutively injected bubbles with bubble injection time of $t_{\mathrm{inj},U} = 75$ ms, a separation time between injections of $t_{\mathrm{sep}} = 50$ ms, and variable lower bubble injection times $t_{\mathrm{inj},L}$ in (a) 1 mm particles and (b) 3 mm particles.

development of the upper bubble is unaffected by the lower bubble injection time. The normalized volume of the lower bubble, however, is much smaller than that of the upper bubble in all cases, indicating that more gas leaks out of the lower bubble during injection. This increased gas leakage can be attributed to increased void fraction in the wake of the upper bubble during the injection of the lower bubble, increasing gas permeability [24] and thus increasing gas leakage. For a lower bubble injection time of 25 ms, the lower bubble decreases in volume as it rises, leading to the collapse of the bubble in the case of 3 mm particles. For larger lower bubble injection times, however, the bubble increases in volume as it rises, likely due to absorption of some gas from the interstitial flow. Despite the fact that the lower bubble collapses in the 25 ms injection case for 3 mm particles, it does not appear that this results in a significant uptake of gas into the upper bubble in this case.

Figure 10 shows the normalized bubble volume at the time of bubble detachment from the orifice versus lower bubble injection time for upper and lower bubbles in beds of 1 and 3 mm particles. There is no clear trend between the normalized bubble injection time and the injection time of the trailing bubble, but the following trends are clear. The bubble volume normalized by volume of gas injected decreases with increasing particle size for the same reason for increasing gas leakage with increasing particle size [23] due to an increased bed permeability as mentioned earlier. Additionally, the normalized bubble volume of the lower bubble is significantly lower than that of the upper bubble in all cases, indicative of increased gas leakage during injection of the second bubble. This

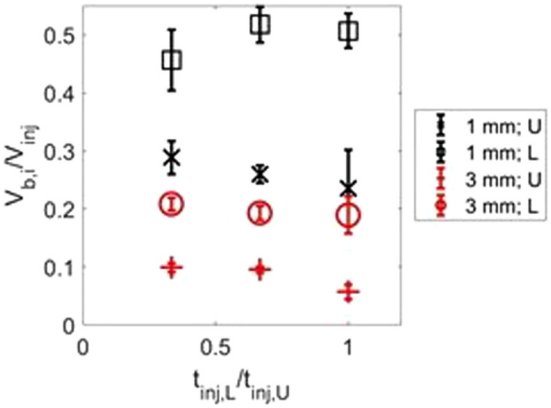

FIG. 10. Normalized bubble volume at the time of bubble breakoff from the injection port for two consecutive bubbles injected for the upper (U) and lower (L) bubble into 1 and 3 mm particles.

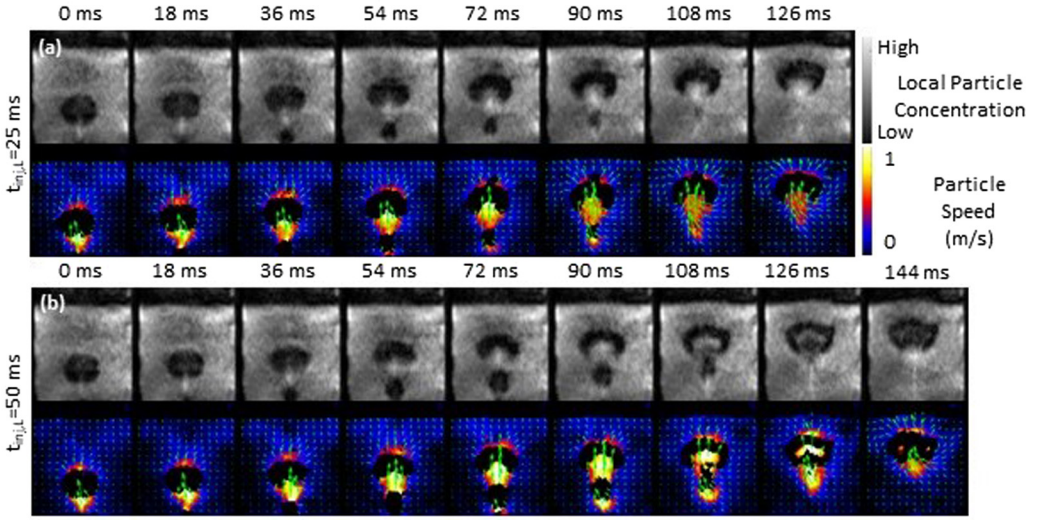

FIG. 11. Time series of images particle signal intensity (upper row) and particle velocity (lower row) for consecutively injected bubbles into incipiently fluidized beds of 3 mm particles with an upper bubble injection time of 75 ms, a separation time of 50 ms between bubble injections, and a lower bubble injection time of (a) 25 and (b) 50 ms.

increased gas leakage could be due to the upward motion of particles in the wake of the upper bubble or a higher void fraction of particles near the orifice during the second bubble injection, due to the influence of the upper bubble.

Figure 11 shows the time series of particle signal intensity (upper row) and particle velocity (lower row) for the consecutive bubble injection cases with 3 mm particles shown in Figs. 8(c) and 8(d). For both injection times of the lower bubble, the lower bubble has fast particle velocities both above and below it, and the lower bubble elongates vertically as it rises, rather than flattening into a spherical-cap shape as seen for isolated bubbles and bubbles rising side by side. The difference in the development of the shape of the lower bubble as compared to all of the other bubbles investigated in this study can be attributed to wake effects from the upper bubble. In the case of the side-by-side bubbles, the left bubble flattens vertically leading to collapse, but the vertical elongation of the lower bubble with an injection time of 25 ms indicates that its collapse must come from another source. We attribute the collapse of the lower bubble in Fig. 11(a) to the increased gas leakage into a high void fraction wake region in combination with the fact that the bubble is smaller than in the case of isolated or side-by-side bubbles due to increased gas leakage during injection. The lower bubble with a 50 ms injection in Fig. 11(b) survives until it coalesces with the upper bubble because it is larger than the 25 ms injection time bubble due to the increased gas injection.

D. Two bubbles injected consecutively through separate ports

Figures 12–14 show the time series of images of particle concentration and velocity for bubbles injected for 25 ms each through different ports with a separation time between injection of the upper and lower bubbles in incipiently fluidized beds of 3 mm particles. For a separation time of 100 ms and a separation distance between injection ports of 80 mm, shown in Fig. 12, the upper bubble rises straight to the bed surface without collapsing. In contrast, the lower bubble moves to the left towards the wake of the upper bubble and decreases in size as it rises until it ultimately collapses. Figure 13 shows similar patterns for bubble behavior for the same case but a separation time between bubbles of 200 ms; the most notable difference is that the lower bubble collapses at a lower position in the bed. Figure 14 shows that for a separation time of 200 ms and a separation distance of 40 mm, the

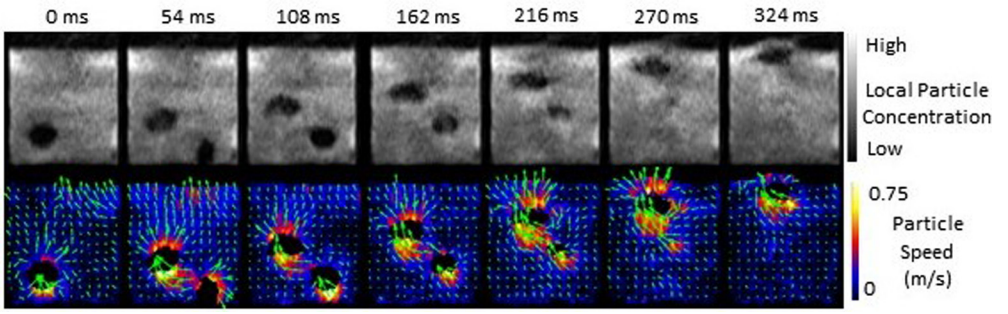

FIG. 12. Time series of images particle signal intensity (upper row) and particle velocity (lower row) for consecutively injected bubbles into incipiently fluidized beds of 3 mm particles with an upper bubble injection time of 25 ms, a separation time of 100 ms between bubble injections, and a lower bubble injection time of 25 ms with a separation distance of 80 mm between injection ports.

lower bubble moves to the left toward the upper bubble and survives to reach the bed surface. For a case with a separation distance of 40 mm and a separation time of 100 ms (not shown), the two bubbles coalesce and then the combined bubble reaches the bed surface without collapsing. Bubble coalescence and survival of the combined bubble was also seen for all equivalent cases with 1 mm particles instead of 3 mm particles.

Since bubbles are not injected through the same port and are injected at different points in time, both the gas channeling mechanism seen for side-by-side bubbles and the increased void fraction in the bubble wake mechanism seen for consecutive bubbles could explain the bubble collapse seen in Figs. 12 and 13. The smaller spatial separation in Fig. 14 as compared to Fig. 13 increases the tendency for the increased void fraction mechanism to cause collapse, rather than the gas channeling mechanism. However, the bubble with the 40 mm separation distance does not collapse, while those with 80 mm separation do collapse, indicating that the gas channeling mechanism causes the collapse seen in Figs. 12 and 13.

E. Nondimensional scaling

With the bubble collapse phenomena demonstrated in this paper and the clear observation that particle size plays a role in these phenomena, it is rational to seek dimensionless parameters

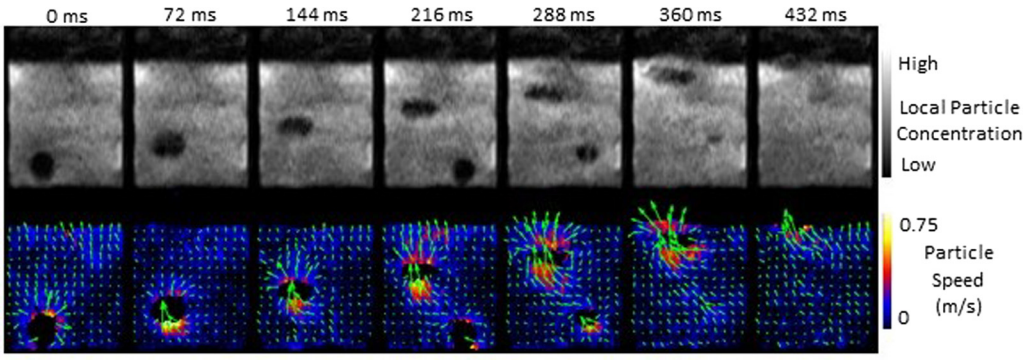

FIG. 13. Time series of images particle signal intensity (upper row) and particle velocity (lower row) for consecutively injected bubbles into incipiently fluidized beds of 3 mm particles with an upper bubble injection time of 25 ms, a separation time of 200 ms between bubble injections, and a lower bubble injection time of 25 ms with a separation distance of 80 mm between injection ports.

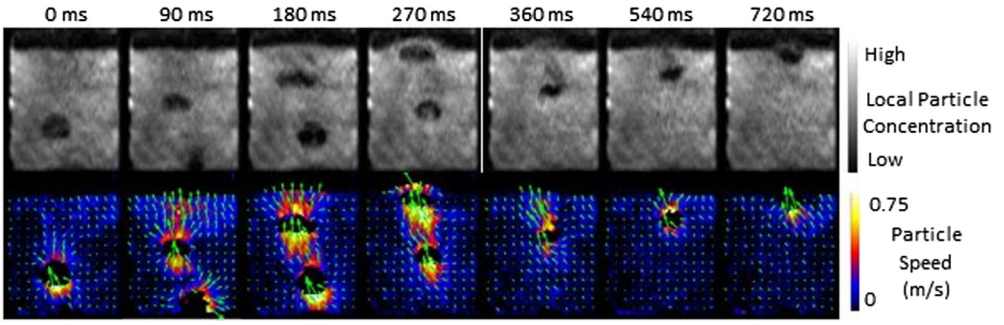

FIG. 14. Time series of images particle signal intensity (upper row) and particle velocity (lower row) for consecutively injected bubbles into incipiently fluidized beds of 3 mm particles with an upper bubble injection time of 25 ms, a separation time of 200 ms between bubble injections, and a lower bubble injection time of 25 ms with a separation distance of 40 mm between injection ports.

involving particle diameter which can create regime maps for bubble collapse phenomena across a wide range of conditions. Unfortunately, with a limited dataset available in this paper, it is not possible to rigorously test the validity of any proposed dimensionless groups governing bubble collapse. Thus, here we will simply discuss potential governing parameters and defer a more in-depth theoretical study validated by a wide range of data to future work.

Since particle diameter has units of length, the simplest nondimensionalization would involve one other parameter with units of length. Bubble collapse is demonstrated to occur in Figs. 4 and 8 for bubbles with smaller initial diameters, but not for larger bubbles, and thus the most obvious dimensionless group would be the ratio of initial bubble diameter to particle diameter, requiring a smaller value to achieve bubble collapse. Also, since bubble interaction is demonstrated to promote bubble collapse, the ratio of separation distance to particle diameter could also be a nondimensional parameter, again expecting that a smaller value of this parameter would lead to bubble collapse. The ability for gas to channel towards a larger bubble and for gas to permeate out of a bubble is also hypothesized here to be related to the bubble collapse phenomena observed. Thus, it is also expected that the effect of particle diameter on gas permeability [24] must also be incorporated into a dimensionless group. Additionally, bubble collapse is also hypothesized to occur due to an inability for gas flowing through the roof of a bubble to maintain the drag force necessary to support the shape of the roof of the bubble during its rise. Thus, the ratio of drag force on a particle in an ensemble of particles to the weight of a particle, including how this varies with particle diameter, is expected to be an important dimensionless group for classifying bubble collapse phenomena.

IV. CONCLUSIONS

MRI measurements showed three cases of anomalous collapse of bubbles injected into incipiently fluidized 3D beds of large particles:

(1) A bubble injected side by side with another bubble collapses, resulting in gas uptake by the neighboring bubble. A mechanism of gas flow channeling to the larger bubble which survives is used to explain this phenomenon.

(2) A lower bubble injected after an upper bubble collapses, which does not appear to result in gas transfer to the upper bubble. A mechanism of increased gas leakage in the dilated wake of the upper bubble has been used to explain this phenomenon.

(3) A lower bubble injected after and to the side of an upper bubble collapses due to the same gas channeling mechanism in (1).

This bubble collapse is anomalous because prior reports of bubble stability have focused on bubbles splitting up rather than collapsing, and the authors are unaware of prior studies of bubble collapse due to bubble interaction. These cases of bubble collapse occur in beds of 3 mm particles,

but not beds of 1 mm particles, indicating that collapse can be attributed to any or all of the following:

(a) smaller bubbles forming in beds of larger particles due to increased gas leakage during bubble injection [23],

(b) increased gas leakage during bubble rise in larger particles,

(c) increased difficulty in small bubbles maintaining a roof of larger particles due to the need for increased gas flow through the roof to lift the particles up due to drag,

(d) increased gas channeling in beds of larger particles because it is easier for gas to move laterally due to the higher permeability to gas flow.

Gas bubbles collapse for the case of interacting bubbles at bubble injection volumes for which isolated bubbles rise to the bed surface without collapse, indicating that bubble interaction can promote bubble collapse. These bubble collapse phenomena represent important challenge problems for theory and computational modeling to predict and seek to further uncover the underlying mechanisms.

ACKNOWLEDGMENT

This work was supported by the Swiss National Science Foundation under Grant No. 200021_153290.

APPENDIX: EFFECT OF THRESHOLD VALUE OF BUBBLE VOLUME

Figure 15 shows the effect of threshold value on the normalized bubble volume versus normalized vertical bubble position for an isolated bubble with a 25 ms injection time in an incipiently fluidized bed of 3 mm particles. The results show that the threshold value changes the quantitative value of the bubble volume, but it does not change the qualitative insights into the decrease, increase, and

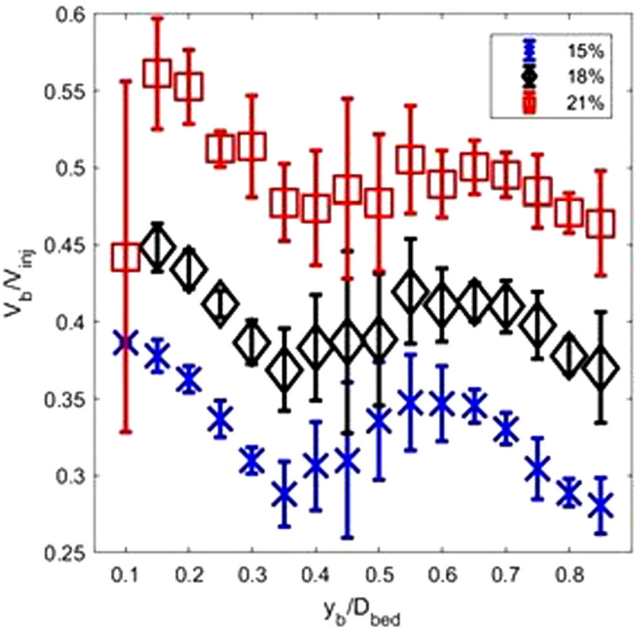

FIG. 15. Effect of threshold value of normalized bubble volume vs normalized vertical position of the bubble for a 25 ms injection time into an incipiently fluidized bed of 3 mm particles. Error bars show the standard deviation from three measurements.

then decrease again in the bubble volume. Thus, we do not consider the insights from this paper to be dependent on the choice of threshold value.

[1] S. Mori and C. Y. Wen, Estimation of bubble diameter in gaseous fluidized beds, AIChE J. **21**, 109 (1975).

[2] R. Clift, J. R. Grace, and M. E. Weber, Stability of bubbles in fluidized beds, Ind. Eng. Chem. Fund. **13**, 45 (1974).

[3] C. R. Müller, J. F. Davidson, J. S. Dennis, P. S. Fennell, L. F. Gladden, A. N. Hayhurst, M. D. Mantle, A. C. Rees, and A. J. Sederman, Real-Time Measurement of Bubbling Phenomena in a Three-Dimensional Gas-Fluidized Bed Using Ultrafast Magnetic Resonance Imaging, Phys. Rev. Lett. **96**, 154504 (2006).

[4] J. S. Halow and P. Nicoletti, Observations of fluidized bed coalescence using capacitance imaging, Powder Technol. **69**, 255 (1992).

[5] T. W. Asegehegn, M. Schreiber, and H. J. Krautz, Investigation of bubble behavior in fluidized beds with and without immersed horizontal tubes using a digital image analysis technique, Powder Technol. **210**, 248 (2011).

[6] C. N. Lim, M. A. Gilbertson, and A. J. L. Harrison, Bubble distribution and behaviour in bubbling fluidised beds, Chem. Eng. Sci. **62**, 56 (2007).

[7] H. T. Bi and J. R. Grace, Flow regime diagrams for gas-solid fluidization and upward transport, Int. J. Multiph. Flow. **21**, 1229 (1995).

[8] D. Bai, E. Shibuya, N. Nakagawa, and K. Kato, Characterization of gas fluidization regimes using pressure fluctuations, Powder Technol. **87**, 105 (1996).

[9] Y. Mawatari, T. Koide, Y. Tatemoto, S. Uchida, and K. Noda, Effect of particle diameter on fluidization under vibration, Powder Technol. **123**, 69 (2002).

[10] R. D. Toomey and H. F. Johnstone, Gaseous fluidization of solid particles, Chem. Eng. Prog. **48**, 220 (1952).

[11] J. R. Grace and R. Clift, On the two-phase theory of fluidization, Chem. Eng. Sci. **29**, 327 (1974).

[12] D. Geldart, Types of gas fluidization, Powder Technol. **7**, 285 (1973).

[13] K. Rahman and C. S. Campbell, Particle pressures generated around bubbles in gas-fluidized beds, J. Fluid Mech. **455**, 103 (2002).

[14] A. Penn, T. Tsuji, D. O. Brunner, C. M. Boyce, K. P. Pruessmann, and C. R. Müller, Real-time probing of granular dynamics with magnetic resonance, Sci. Adv. **3**, e1701879 (2017).

[15] C. M. Boyce, A. Penn, K. P. Pruessmann, and C. R. Müller, Magnetic resonance imaging of gas–solid fluidization with liquid bridging, AIChE J. **64**, 2958 (2018).

[16] A. Penn, C. M. Boyce, T. Kovar, T. Tsuji, K. P. Pruessmann, and C. R. Müller, Real-time magnetic resonance imaging of bubble behavior and particle velocity in fluidized beds, Ind. Eng. Chem. Res. **57**, 9674 (2018).

[17] C. M. Boyce, A. Penn, M. Lehnert, K. P. Pruessmann, and C. R. Müller, Effect of liquid bridging on bubbles injected into a fluidized bed: A magnetic resonance imaging study, Powder Technol. **343**, 813 (2019).

[18] C. M. Boyce, A. Penn, M. Lehnert, K. P. Pruessmann, and C. R. Müller, Magnetic resonance imaging of single bubbles injected into incipiently fluidized beds, Chem. Eng. Sci. **200**, 147 (2019).

[19] C. M. Boyce, A. Penn, M. Lehnert, K. P. Pruessmann, and C. R. Müller, Wake volume of injected bubbles in fluidized beds: a magnetic resonance imaging velocimetry study, Powder Technol. (to be published).

[20] C. M. Boyce, A. Penn, A. Padash, M. Lehnert, K. P. Pruessmann, and C. R. Müller, An alternating bubble pattern arising in fluidized beds due to jet interaction: a magnetic resonance imaging study (unpublished).

[21] M. K. Stehling, R. Turner, and P. Mansfield, Echo-planar imaging: Magnetic resonance imaging in a fraction of a second, Science. **254**, 43 (1991).

[22] P. T. Callaghan, *Principles of Nuclear Magnetic Resonance Microscopy* (Oxford University Press, Oxford, 1991).
[23] H. S. Caram and K.-K. Hsu, Bubble formation and gas leakage in fluidized beds, Chem. Eng. Sci. **41**, 1445 (1986).
[24] J. Kozeny, About capillary flow of water in soil, Proc. Acad. Sci. Vienna **136**, 271 (1927).